Advances in reducing radiometric miscalibration – application for hyperspectral push-broom sensors

Christian Rogass[1], Christian Mielke[1], Daniel Scheffler[1], Nina K. Boesche[1],

Christin Lubitz[1], Maximilian Brell[1], Daniel Spengler[1] and Karl Segl[1]

1. Helmholtz Centre Potsdam GFZ German Research Centre for Geosciences, Section Remote Sensing, Potsdam, Germany; emails: christian.rogass, christian.mielke,daniel.scheffler,nina.boesche,christin.lubitz,maximilian.brell,Daniel.spengler, karl.segl (@gfz-potsdam.de)

ABSTRACT

Data takes of hyperspectral imagers are of increasing demand in Earth Observation related applications. As for other remote sensing techniques this requires precise pre-processing comprising of radiometric, spectral and geometric distortion reductions. One of these steps is radiometric scaling to transform recorded digital number to radiance. For this, laboratory assessed mathematical relations between required radiance and recorded digital number (gain) and short-term measurements of dark current variations (offset) during operation are incorporated. Due to changes in the sensor system, which include thermal imbalance and mechanical stress gain and offset may vary over time. The result of this is visually perceptible as along-track striping noise after radiometric calibration. In this work, a new approach is presented that enables fast, highly precise and parameter-free destriping of uncorrelated striping noise that enhances the radiometric accuracy of hyperspectral push-broom data takes, and, hence, improves the outputs of succeeding applications. It is part of the existing ROME (Reduction of Miscalibration Effects) framework and is based on a noise-perpendicular gradient minimization technique. The performance was tested and compared to four state-of-the-art algorithms using artificially degraded hyperspectral whisk-broom scenes from a HyMAP campaign over Germany, two AISA scenes over Germany and two EO-1 Hyperion scenes over Namibia. Proposed approach clearly outperforms all other tested approaches even in low SNR scenarios like close to atmospheric absorption bands. On average a destriping accuracy of 99.75 % can be achieved having 3σ of only 1 % and, thus, it has been integrated into the state-of-the-art ROME framework that becomes a standard inside hyperspectral pre-processing chains.

INTRODUCTION

Remote sensing acquisitions often serve as a basis for geospatial applications. Especially imaging spectroscopy becomes more and more important because continuous pixel spectra enable the differentiation of surface cover materials. Modern sensors that utilize the push broom technology offer a broad applicability through the variable integration time but have to be carefully radiometrically calibrated. This is usually performed in special laboratories. Estimated calibration sets are then used to transform the raw hyperspectral data cube into physics based units such as at-sensor-radiance that generally builds the base for any application. If the characteristics of the detectors change over time and do not temporally coincide with last laboratory calibration, then visual perceptible along-track stripes occur in the acquisitions that aggravates succeeding applications. However, in this work a new approach is presented that significantly reduce stripes. It relates to human perception through its global gradient minimization principle and clearly outperforms inspected current state-of-the-art destriping approaches. It has been evaluated using data sets of three different hyperspectral sensors – HyMAP, AISA Dual and EO-1 Hyperion - for which ground-truth was partly available. In the following the basic concepts and related results are briefly presented.

 ISBN 978-83-63245-65-8, DOI: 10.12760/03-2014-09, Zagajewski B., Kycko M., Reuter R. (eds.)

MATERIALS

In this work a set of hyperspectral images has been used for the evaluation of the proposed algorithm. Those set comprises three atmospherically corrected airborne HyMAP [1] scenes, two radiometrically corrected spaceborne EO-1 Hyperion [2] scenes and two radiometrically corrected airborne AISA Dual [3] scenes. The HyMAP scenes were acquired over Potsdam (2004), Dresden (2003) and Berlin (2005) in Germany. The Hyperion scenes were acquired over the Haib River Complex crossing Namibia and the Republic of South Africa in 2013 and 2014. The AISA scenes were acquired over the Fichtwald region in Germany in 2010. The HyMAP acquisitions have been utilized as test bed for destriping of artificial stripe degradations, because whisk broom data takes are mostly unaffected by dark current variations induced stripes. Those scenes have been atmospherically corrected using ATCOR [4] before degradation. Then, each band of each scene has been independently and artificially degraded by adding White Gaussian Noise (WGN) that was generated as proposed in [5], whereas different noise degradation levels (0.1 %, 0.5 %, 1 % and 5 %) have been realized resulting in 1536 different striping scenarios (4 noise levels, 3 HyMAP images, 128 bands; figure 2). For each scenario ground-truth was available as original image that then served as evaluation basis. All other hyperspectral scenes from AISA and Hyperion remained unchanged due to their existing stripe degradation as shown in figure 1 and 2.

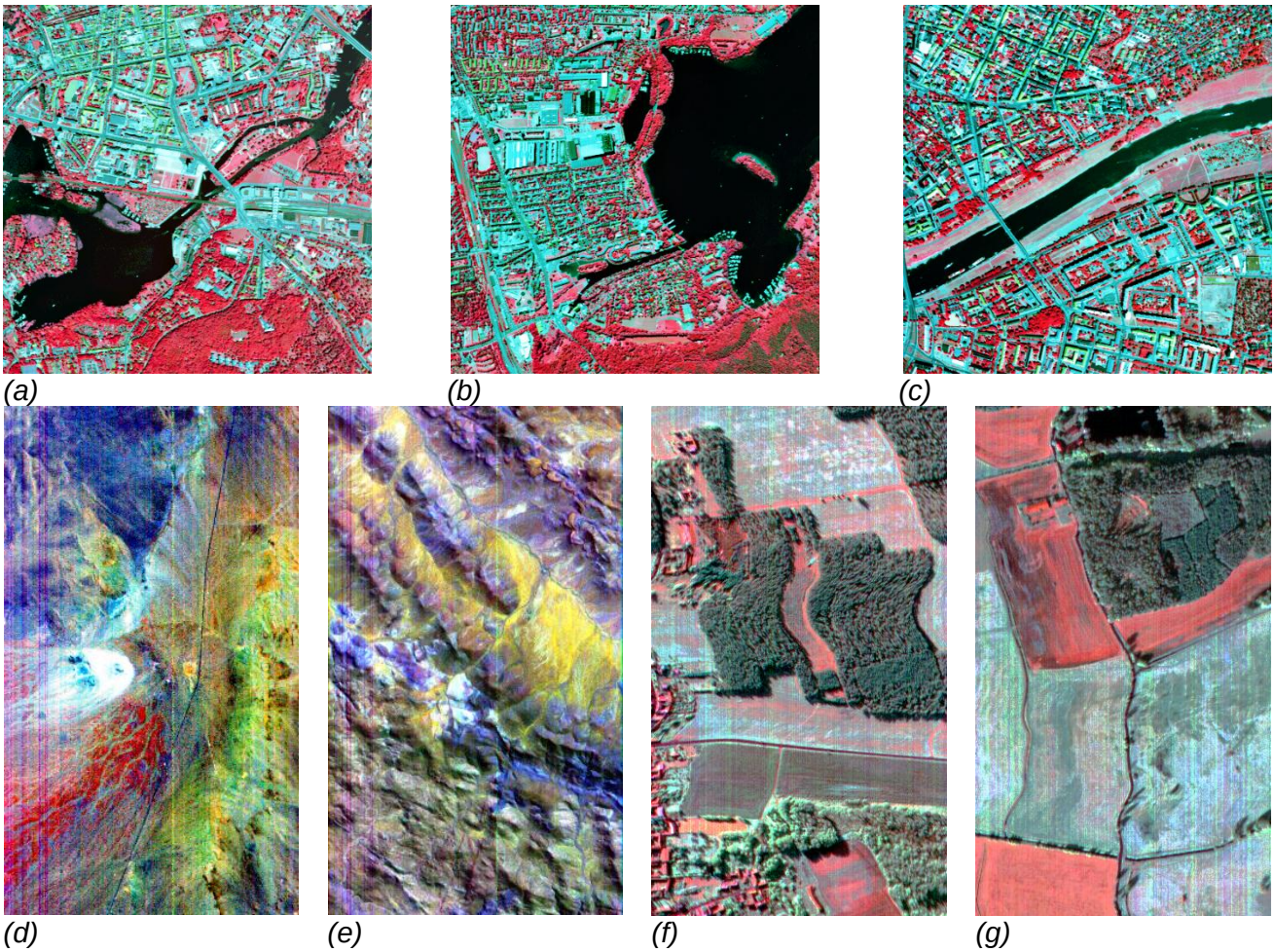

Figure 1. False colored representations of subsets of HyMAP acquisitions over (a) Potsdam (CIR: Red 864.5 nm, Green 652.6 nm, Blue 546.3 nm), (b) Berlin (CIR as in (a), (c) Dresden and of subsets of Hyperion acquisitions over (d-e) the Haib River Complex (Red 2304.71 nm, Green

915.23 nm, Blue 447.17 nm), and subsets of AISA acquisitions over the Fichtwald region (f) and (g) (Red 1574.37 nm, Green 964.39 nm, Blue 730.05 nm)

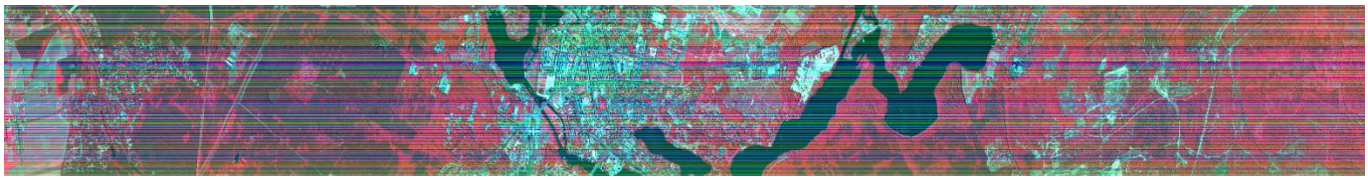

Figure 2. False colored scene of a HyMAP acquisition over Potsdam (CIR: Red 864.5 nm, Green 652.6 nm, Blue 546.3 nm) that was artificially degraded with 5% dark current variation

METHODS

The destriping approach consists of several modules that are shown in figure 3, whereas this approach assumes that along-track stripes induce artificial across-track gradients which have to be minimized.

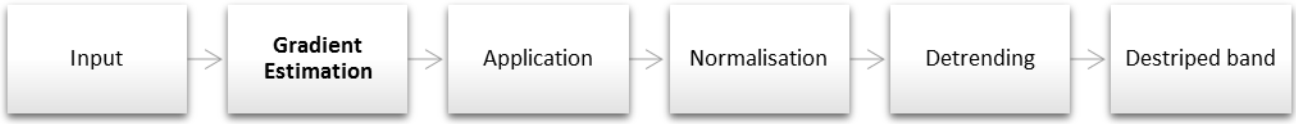

Figure 3. Destriping scheme

The following equation serves as basis for succeeding considerations:

$$\underline{im} = \underline{im}_s - \underline{s} \tag{1}$$

where $\underline{im}$ is one band of the at-sensor radiance image without stripes, $\underline{im}_s$ is one band of the real at-sensor radiance image and $\underline{s}$ is the striping noise matrix of one band. This would then lead to the following equation coping with the gradient minimization constraint:

$$\int med_y \left| \frac{\partial\, \underline{im} - \underline{im}_s}{\partial x} \right| dx = \int med_y \left| \frac{\partial\, \underline{s}}{\partial x} \right| dx = \underline{s} \tag{2}$$

where med_y is the along track median. This is valid for along-track stripes, because their along-track median becomes their own argument that can be represented as integral of its derivative or, hence, the stripe pattern itself. To solve equation 2, it is necessary to assess $\frac{\partial\, \underline{im}}{\partial x}$ e.g. as high-pass of $\frac{\partial\, \underline{im}_s}{\partial x}$. Additionally, any estimated stripe matrices have to be mean normalized in order to have a zero mean property as the dark current variations (thermal Gaussian noise). Also remaining long-wave trends have to be reduced, e.g. by applying the approach of [6].

In addition to the proposed method several other methods have been tested. Those were the current state-of-the-art approaches of [7–11]. To evaluate the results for the artificial HyMAP degradations three performance indicators have been selected. Those were the Peak-Signal-To-Noise Ratio (PSNR) [6,12], the Modified Structural Similarity Index Measure (MSSIM) [12–14] and the column correlation or spectral correlation. To evaluate the AISA and Hyperion images a new performance indicator has been defined. It is the Absolute Average of Highpass of Differences (AAHPD). The related equation is given in the following to:

© EARSeL and University of Warsaw, 2014, ISBN 978-83-63245-65-8, DOI: 10.12760/03-2014-09, Zagajewski B., Kycko M., Reuter R. (eds.)

$$AAHPD = \left| \frac{\sum_{cols} \frac{\sum_{rows} \underline{diff} - \underline{diff} \oplus \underline{fil}_3}{\sum_{rows} row}}{\sum_{cols} col} \right| \quad (3)$$

whereas $\underline{diff}$ represents smoothed difference between the destriping result and the original image using the 3x3 filter $\underline{fil}_3$, col the detector element or across track position, row the scan line number (y or along track scan line position or time) and $\otimes$ is the dyadic product.

RESULTS AND DISCUSSION

In the following the results are briefly presented and discussed. All objectively derived evaluation results have been averaged and are given in table 1. Additionally, the three-sigma probability estimate 3σ has been computed to account for the variation or volatility of the indicator.

Table 1: Averaged results for all images

Approach / Indicator	M1	M2	M3	M4	M5	M6
PSNR [%] (3σ)	99.92 (0.30)	97.09 (11.22)	97.20 (14.45)	83.50 (19.97)	99.81 (4.56)	85.87 (27.54)
SSIM [%] (3σ)	99.58 (1.43)	93.40 (29.99)	93.43 (29.92)	80.57 (46.47)	95.68 (22.79)	65.94 (24.07)
Spectral Correlation [%] (3σ)	99.96 (0.4)	91.34 (11.54)	86.19 (8.70)	78.65 (15.73)	93.77 (6.72)	95.77 (7.23)
Average [%] (3σ)	**99.82 (0.71)**	**93.94 (17.58)**	**92.27 (17.69)**	**79.71 (27.39)**	**95.13 (11.35)**	**80.66 (19.61)**
AAHPD / Hyperion [#] (3σ)	0.00004 (0.0029)	0.00028 (0.0021)	0.00034 (5.5623)	0.00084 (0.3825)	0.00060 (0.0031)	0.00166 (0.0136)
AAHPD / AISA [#] (3σ)	0.02311 (1.3208)	0.0634 (1.3666)	0.18276 (157.7)	0.05955 (1.3317)	0.06011 (1.4045)	0.09223 (1.8410)
AAHPD [#] (3σ)	**0.00962 (0.6476)**	**0.03144 (0.6557)**	**0.04128 (59.052)**	**0.02516 (0.9894)**	**0.02733 (0.6759)**	**0.031 (0.7650)**

M1: Proposed approach
M2: Rogass et al. (2012)
M3: Goodenough et al. (2003) and Datt et al. (2003)
M4: Staenz et al. (2003)
M5: Pande-Chhetri and Abd-Elrahman (2011)
M6: Pande-Chhetri and Abd-Elrahman (2013)

According to table 1 the proposed approach clearly outperforms all other approaches. Second best approach is the approach of [10]. Third best approach is [7]. However, the approach of [8,9] also provides good results if visual perception is additionally used for evaluation as exemplarily shown in figure 4. Hence, visual perception has been integrated as subjective evaluation criterion.

© EARSeL and University of Warsaw, 2014, ISBN 978-83-63245-65-8, DOI: 10.12760/03-2014-09, Zagajewski B., Kycko M., Reuter R. (eds.)

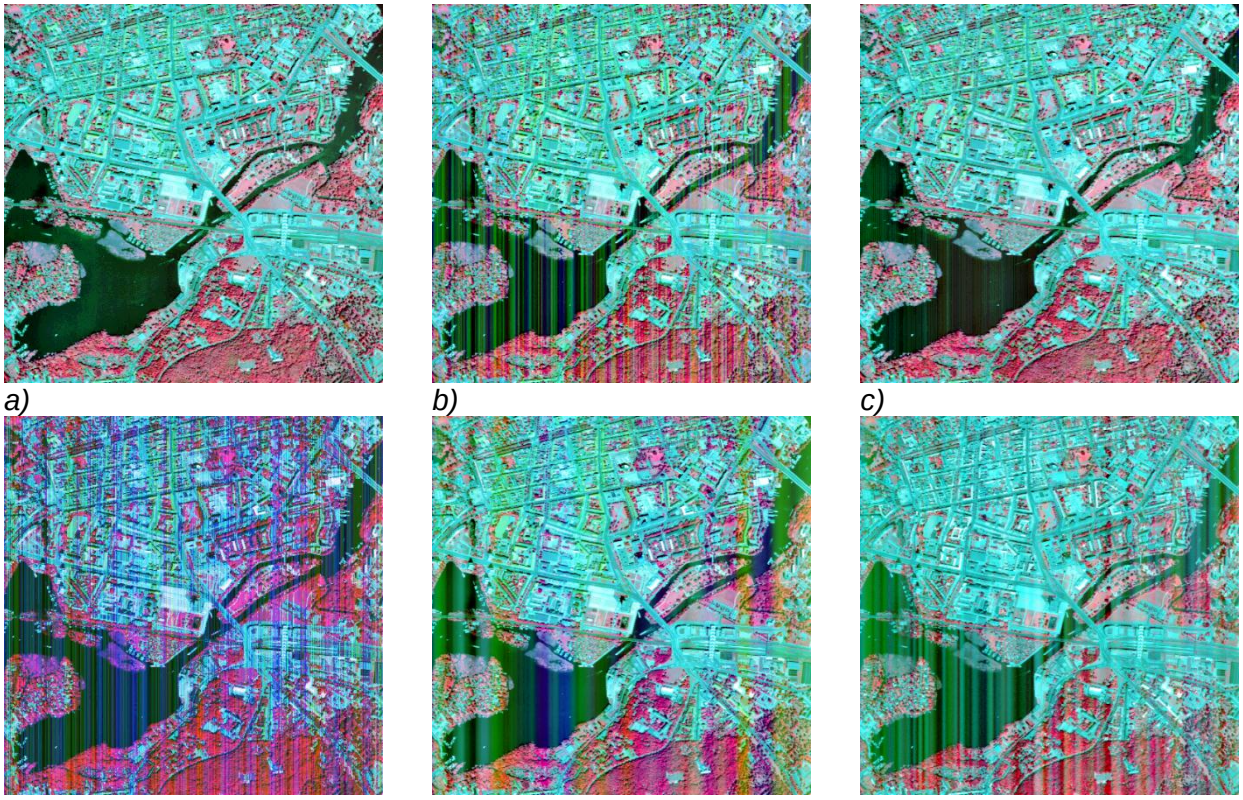

Figure 4: Subsets of one HyMAP scene as false color composites of the destriping results of (a) the proposed approach, (b) Rogass et al. 2012, (c) Goodenough et al. 2003 and Datt et al. 2003, (d) Staenz et al. 2002, (e) Pande-Chhetri et al. 2011 and (f) Pande-Chhetri et al. 2013

If subjective evaluations are integrated into the evaluation scheme as ranking, then all other applied evaluation metrics have to be also ranked as in table 2.

Table 2: Overall averaged performance ranking

Overall performance ranking						
Approach / Indicator	M1	M2	M3	M4	M5	M6
PSNR [#]	**1**	4	**3**	6	**2**	5
SSIM [#]	**1**	4	**3**	5	**2**	6
Spectral Correlation [#]	**1**	4	5	6	**3**	**2**
Visual comparison HyMAP [#]	**1**	**3**	**2**	6	4	5
Median AAHPD / Hyperion [#]	**1**	**2**	**3**	5	4	6
Median AAHPD / AISA [#]	**1**	4	6	**2**	**3**	5
Visual comparison Hyperion [#]	**1**	**3**	**1**	5	**2**	4
Visual comparison AISA [#]	**1**	5	**1**	**3**	4	**2**
Average [#] **(Σ all, Σ objectively)**	**1** **(8, 5)**	3 (3) (29, 18)	**2 (4)** **(24, 20)**	5 (5) (38, 24)	2 (2) (24, 14)	4 (6) (35, 24)

According to table 2 the proposed approach outperforms all other inspected approaches, but second best approach are now the common approach of [8,9] and the approach of [10].

© EARSeL and University of Warsaw, 2014, ISBN 978-83-63245-65-8, DOI: 10.12760/03-2014-09, Zagajewski B., Kycko M., Reuter R. (eds.)

CONCLUSION

In this work a new concept for efficient destriping of uncorrelated striping noise have been proposed. It works with different sensors and clearly outperforms all other inspected approaches. It will substitute current algorithms of the ROME framework (Reduction of Miscalibration Effects, [6]) that widely used in the past. However, future tests will include more different push broom acquisitions as well as along-track gradients.

ACKNOWLEDGEMENTS

This work was funded by the German Federal Ministry of Economics and Technology (BMWI 506 50EE1012/EnMAP) within the framework of EnMAP (Environmental Mapping and Analysis Program). We thank the U.S. Geological Survey's Earth Resources Observation and Science (EROS) Center for providing image samples.

REFERENCES

1. Cocks, T.; Jenssen, R.; Stewart, A.; Wilson, I.; Shields, T. The HyMapTM airborne hyperspectral sensor: the system, calibration and performance. In 1st EARSEL Workshop on Imaging Spectroscopy, Zurich, Switzerland; 1998; pp. 37–42.

2. Pearlman, J.; Carman, S.; Segal, C.; Jarecke, P.; Clancy, P.; Browne, W. Overview of the Hyperion Imaging Spectrometer for the NASA EO-1 mission. In Geoscience and Remote Sensing Symposium, 2001. IGARSS ’01. IEEE 2001 International; 2001; Vol. 7, pp. 3036–3038 vol.7.

3. Spectral Imaging aisaDUAL - Specim http://www.specim.fi/index.php/products/airborne/aisadual (accessed Feb 17, 2014).

4. Richter, R.; Schläpfer, D. Geo-atmospheric processing of airborne imaging spectrometry data. Part 2: Atmospheric/topographic correction. Int. J. Remote Sens. 2002, 23, 2631–2649.

5. Box, G.; Muller, M. E. A note on the generation of random normal deviates. Ann. Math. Stat. 1958, 29, 610–611.

6. Rogass, C.; Spengler, D.; Bochow, M.; Segl, K.; Lausch, A.; Doktor, D.; Roessner, S.; Behling, R.; Wetzel, H. U.; Kaufmann, H. Reduction of radiometric miscalibration - applications to pushbroom sensors. Sensors 2011, 11, 6370–6395.

7. Rogass, C.; Spengler, D.; Bochow, M.; Segl, K.; Lausch, A.; Doktor, D.; Roessner, S.; Behling, R.; Wetzel, H. U.; Urata, K.; Hueni, A.; Kaufmann, H. A Contribution to the Reduction of Radiometric Miscalibration of Pushbroom Sensors. In Remote Sensing - Advanced Techniques and Platforms; Escalante-Ramirez, B., Ed.; InTech, 2012; pp. 151–170.

8. Goodenough, D. G.; Dyk, A.; Niemann, K. O.; Pearlman, J. S.; Chen, H.; Han, T.; Murdoch, M.; West, C. Processing Hyperion and ALI for forest classification. IEEE Trans. Geosci. Remote Sens. 2003, 41, 1321–1331.

9. Datt, B.; McVicar, T. R.; Van Niel, T. G.; Jupp, D. L. B.; Pearlman, J. S. Preprocessing EO-1 Hyperion hyperspectral data to support the application of agricultural indexes. IEEE Trans. Geosci. Remote Sens. 2003, 41, 1246–1259.

10. Pande-Chhetri, R.; Abd-Elrahman, A. De-striping hyperspectral imagery using wavelet transform and adaptive frequency domain filtering. ISPRS J. Photogramm. Remote Sens. 2011, 66, 620–636.

11. Pande-Chhetri, R.; Abd-Elrahman, A. Filtering high-resolution hyperspectral imagery in a maximum noise fraction transform domain using wavelet-based de-striping. Int. J. Remote Sens. 2013, 34, 2216–2235.

 ISBN 978-83-63245-65-8, DOI: 10.12760/03-2014-09, Zagajewski B., Kycko M., Reuter R. (eds.)

12. Wang, Z.; Bovik, A. C. Mean squared error: Love it or leave it? A new look at Signal Fidelity Measures. IEEE Signal Process. Mag. 2009, 26, 98–117.

13. Wang, Z.; Bovik, A. C.; Sheikh, H. R.; Simoncelli, E. P. Image quality assessment: From error visibility to structural similarity. Image Process. IEEE Trans. On 2004, 13, 600–612.

14. Tsai, F.; Chen, W. W. Striping Noise Detection and Correction of Remote Sensing Images. IEEE Trans. Geosci. Remote Sens. 2008, 46, 4122–4131.